Simulation Analysis of Main Bearing Vibration Characteristics of Wind Turbine

Liang Xuan[1,2(✉)], Ao Shen[1,2], Xiaochi He[1,2], Shuai Dong[1,2], and Jiaxin Dong[1,2]

[1] State Key Laboratory of Precision Blasting, Jianghan University, Wuhan 430056, China
xuanl@jhun.edu.cn

[2] School of Smart Manufacturing, Jianghan University, Wuhan 430056, China

Abstract. The operating condition of the main bearing of the wind turbine directly affects the stability of the whole wind turbine, and it is crucial to analyze the vibration characteristics of the main bearing. In this paper, not only the theoretical analysis of the main bearing's inherent frequency was carried out, but also the vibration characteristics under different constraints are studied by the finite element analysis method, and the first six orders of inherent frequency and vibration pattern of the bearing are listed, and it is found that the deformation is mainly concentrated in the axial direction. Further, the axial vibration simulation experiments of the constrained radial direction were carried out, and the maximum deformation in the axial direction was obtained as 24.9% of the thickness of the main bearing. It provides a theoretical basis for the selection of sensor parameters (range and signal sampling frequency) for further main bearing operation condition monitoring.

Keywords: Wind power spindle bearing · Modal Analysis · Vibration characteristics · Finite element simulation

1 Introduction

As one of the key components of the wind turbine [1], the main bearing is subjected to dynamic loads of different directions and magnitudes in complex environments, and its stable operation directly affects the performance of the whole wind turbine unit [2]. During the operation of the main bearing of the wind turbine, different vibration characteristics are generated under different loads. To ensure the stable operation of the main bearing and to improve its vibration resistance, its vibration characteristics must be analyzed to ensure its stable and reliable operation [3]. The assembly diagram of the main bearing of the wind turbine is shown in Fig. 1.

There are many theoretical analysis methods to study the vibration pattern of wind turbine main shaft bearings, such as the theoretical force state analysis method, dynamics analysis method, finite element modal analysis method, etc. can obtain the vibration characteristics of the main bearing [4]. In this paper, the modal analysis of the main bearing of the wind turbine is carried out by the finite element analysis method, and its corresponding inherent frequency and deformation are obtained according to the vibration pattern of the main bearing under different load states [5].

F. Chu and Z. Qin (Eds.): IFToMM 2023, MMS 139, pp. 447–461, 2024.
https://doi.org/10.1007/978-3-031-40455-9_36

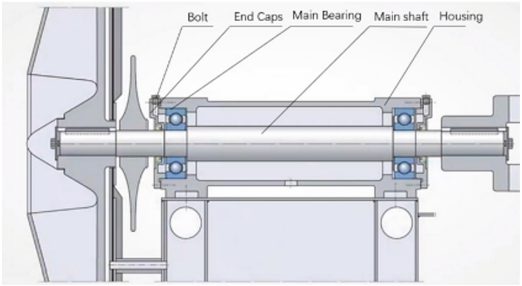

Fig. 1. Wind turbine assembly diagram

In this paper, not only the theoretical analysis of the main bearing inherent frequency was carried out, but also the vibration characteristics under different constraints are studied through the finite element analysis method to provide a theoretical basis for further development of the selection of the main bearing operating condition monitoring sensor parameters.

2 Theoretical Analysis of the Inherent Frequency of the Main Bearing

During the movement of a bearing, an impact may be generated between the rolling element and the inner and outer rings, which in turn causes vibration of the bearing itself. The size of the inherent frequency of the bearing is determined by the shape and quality of the component itself as well as the stiffness of the bearing component itself, independent of the service conditions and operating speed of the rolling bearing.

The formula for calculating the inherent frequency of a rolling element made of steel is as follows:

$$f_{ball} = \frac{0.424}{d_b}\sqrt{\frac{E}{2\rho}} \tag{1}$$

where: d_b is the diameter of the rolling body, ρ is the density of the rolling body material, E is the modulus of elasticity of the rolling body.

The inner ring inherent frequency calculation formula is as follows:

$$f_{in} = 9.40 \times 10^5 \times R_i^2\sqrt{\frac{EI}{M}} \times \frac{n\left(n^2-1\right)}{\sqrt{n^2+1}} \tag{2}$$

The inherent frequency of the outer ring is calculated by the following formula:

$$f_{out} = 9.40 \times 10^5 \times R_o^2\sqrt{\frac{EI}{M}} \times \frac{n\left(n^2-1\right)}{\sqrt{n^2+1}} \tag{3}$$

where Rx (x = i,o) is the radius from the inner and outer ring rotation axis to the neutral axis, n is the order of the intrinsic frequency, n = 1,2,3,… I is the moment of inertia

of the circular section around the neutral axis, and M is the mass per unit length of the circular [6].

The same bearing E, I, M and other parameters of the same value, take the same inherent frequency order n, because the outer ring radius Ro is greater than the inner ring radius Ri, so the same order of the outer ring inherent frequency is greater than the inner ring inherent frequency, the stability of the outer ring of the bearing more need to monitor.

3 Establishment of Finite Element Model

3.1 Model Building

In this paper, a bearing with an inner diameter of 300 mm, an outer diameter of 420 mm, a thickness of 56 mm, and model number 61960 was used for the simulation experiments. As Fig. 2 Fig. 3 shows the 3D model of the main bearing of the wind turbine established by Solidworks software, the cage was removed for modal analysis in the simulation experiment [7].

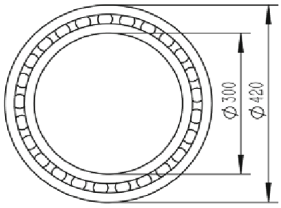

Fig. 2. Dimensional drawing of main bearing

Fig. 3. 3D model of main bearing

The 3D assembly drawing model of the main bearing in Solidworks was imported into ANSYS Workbench 18.0 in x_t format.

Since the main bearing of the wind turbine is an assembly, contact settings are required between the parts, and the bonding method between the inner and outer rings of the main bearing and the rollers is selected as bound (bonded) contact [8].

3.2 Adding Material Properties

The main bearing of the wind turbine is made of common bearing steel AISI52100 (GCr15), where Young's modulus E is 2×10^5 MPa, Poisson's ratio is 0.3, and density is 7850 kg/m^3.

3.3 Mesh Division

In the process of finite element simulation, the quality of meshing directly affects the accuracy of the solution [9]. In this paper, automatic meshing is used, the global cell size of the meshing is set to 5mm and the smoothness is set to Medium. Following the above

steps, the 3D solid cell model of the main bearing of the wind turbine is transformed into a 3D finite element cell model, which contains a total of 134,544 nodes and 310,043 cells. Figure 4 shows the 3D finite element cell model after meshing.

Fig. 4. 3D finite element cell model

3.4 Force Analysis

The main bearing of the wind turbine is mounted on the main shaft, the main shaft is fixed with the inner ring of the main bearing, the shoulder of the main shaft, and the end face of the end cap clamp both sides of the inner ring of the main bearing, the housing restricts the radial movement of the outer ring of the main bearing, the end face of the end cap and the side of the housing restricts the axial movement of the outer ring of the main bearing. In summary, the main bearing needs to bear the load in both radial and axial directions, this paper uses the main bearing inner ring fixed, and the main bearing outer ring to apply different sizes of axial force and radial force restraint methods.

4 Modal Analysis

4.1 No-Load Modal Analysis

Determination of Working Conditions and Loads
The no-load modal analysis of the main bearing fixes only the inner surface of the inner ring of the main bearing, and its no-load simulation experimental model constraint is shown in Fig. 5.

Simulation Results and Analysis
In this paper, the first six orders of intrinsic frequencies and vibration patterns are selected for analysis and comparison, and since no load acts on the main bearing, the vibration patterns are only the relative values associated with free vibration [11]. Table 1 shows the simulation data, and the simulation results are shown in Fig. 6.

As shown in Fig. 6, the first-order mode is the torsional vibration along the axial direction of the bearing; the second, third, and fourth orders are the bending vibration along the radial direction of the bearing; the fifth and sixth orders are the bending-torsional coupling vibration. As can be seen from the first six-order mode vibration

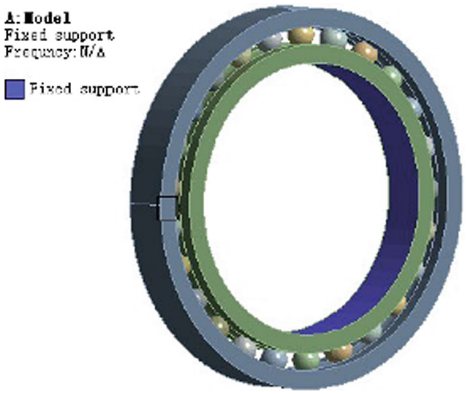

Fig. 5. No-load simulation experimental model constraint diagram

Table 1. No-load simulation experimental inherent frequency and maximum displacement

Number of steps	Frequency /Hz	Maximum displacement /mm	Vibration diagram
First step	2867.8	10.428	Figure 6-(a)
Second step	2994.4	23.689	Figure 6-(b)
Third step	3021.0	19.787	Figure 6-(c)
Fourth step	3120.6	19.909	Figure 6-(d)
Fifth step	3129.6	20.548	Figure 6-(e)
Sixth step	3224.6	17.424	Figure 6-(f)

diagram, the maximum displacement is produced in the second-order mode, and the outer ring of the bearing is twisted in the radial direction, with a maximum displacement of 23.689 mm, corresponding to a frequency of 2994.4Hz.

RATIO (ratio) indicates the ratio of the vibration mode participation coefficient to the first-order vibration mode participation coefficient. In the PARTICIPATION FACTOR CALCULATION information table, the order with the value of 1 is the direction in which the vibration change of the model at that intrinsic frequency occurs mainly.

From the information of the no-load simulation experimental solution scheme in Table 2, it can be seen that the first-order mode has the largest deformation in the Y-direction, Z-direction, and around the X-axis, and the corresponding fixed frequency is 2867.82 Hz. The sixth-order mode has the largest deformation in the X-direction and around the Y-direction, and the corresponding fixed frequency is 3224.64 Hz. The fifth-order mode has the largest deformation around the Z-axis, and the corresponding fixed frequency is 3129.63 Hz.

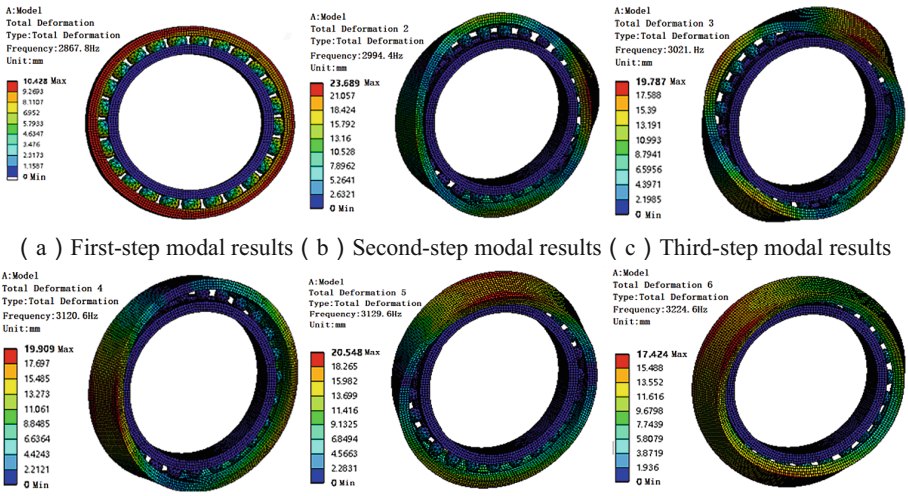

(a) First-step modal results (b) Second-step modal results (c) Third-step modal results

(d) Fourth-step modal results (e) Fifth-step modal results (f) Sixth-step modal results

Fig. 6. The first six orders of mode vibration diagram

4.2 Loading Modal Analysis

Determination of Working Conditions and Loads

After fixing the inner surface of the inner ring of the model bearing, different magnitudes of radial force Fr and axial force Fa need to be applied according to the actual load situation.

The simulation experimental value of the equivalent dynamic load (P/N) is determined by combining the actual load on the main bearing of the wind turbine and the bearing load range of the model. Thus, the radial force and axial force are allocated according to Eq. (4) and the determined equivalent dynamic load.

$$P = f_d(XF_r + YF_a) \tag{4}$$

where the equivalent dynamic load P is in N, X, and Y are the radial dynamic load coefficient and axial dynamic load coefficient, Fr is the radial load and Fa is the axial load, both in N.

For the steady state bearing without shock, check the table to take the load coefficient of 1. Check the table to take the radial dynamic load coefficient X as 0.56, axial dynamic load coefficient Y as 2.0, and judgment coefficient e as 0.22.

Table 2. No-load simulation experiment solving scheme information

Number of steps	Frequency /Hz	RATIO
First step	2867.8	0.009869
Second step	2994.4	0.049493
Third step	3021.0	0.009418
Fourth step	3120.6	0.157150
Fifth step	3129.6	0.013563
Sixth step	3224.6	1.000000

(a) PARTICIPATION FACTOR CALCULATION_X DIRECTION

Number of steps	Frequency /Hz	RATIO
First step	2867.8	1.000000
Second step	2994.4	0.008867
Third step	3021.0	0.046015
Fourth step	3120.6	0.093526
Fifth step	3129.6	0.044834
Sixth step	3224.6	0.018820

(b) PARTICIPATION FACTOR CALCULATION_Y DIRECTION

Number of steps	Frequency /Hz	RATIO
First step	2867.8	1.000000
Second step	2994.4	0.023414
Third step	3021.0	0.014787
Fourth step	3120.6	0.004673
Fifth step	3129.6	0.128051
Sixth step	3224.6	0.037039

(c) PARTICIPATION FACTOR CALCULATION_Z DIRECTION

(*continued*)

Table 2. (*continued*)

Number of steps	Frequency /Hz	RATIO
First step	2867.8	1.000000
Second step	2994.4	0.004179
Third step	3021.0	0.002828
Fourth step	3120.6	0.006335
Fifth step	3129.6	0.001344
Sixth step	3224.6	0.007495

(d) PARTICIPATION FACTOR CALCULATION_ROTX DIRECTION

Number of steps	Frequency /Hz	RATIO
First step	2867.8	0.012470
Second step	2994.4	0.090974
Third step	3021.0	0.034618
Fourth step	3120.6	0.398414
Fifth step	3129.6	0.295273
Sixth step	3224.6	1.000000

(e) PARTICIPATION FACTOR CALCULATION_ROTY DIRECTION

Number of steps	Frequency /Hz	RATIO
First step	2867.8	0.012810
Second step	2994.4	0.007591
Third step	3021.0	0.004083
Fourth step	3120.6	0.526109
Fifth step	3129.6	1.000000
Sixth step	3224.6	0.243918

(f) PARTICIPATION FACTOR CALCULATION_ROTZ DIRECTION

The basic dynamic load rating Cr of the bearing model 61960 is 270 KN and the basic static load rating Cor is 370 KN, so this simulation experiment uses radial force 240 KN and axial force 32.8 KN, i.e., the equivalent dynamic load P is 200 KN group simulation experiment as a comparison test for analysis. The model constraint diagram when loading radial force and axial force simultaneously is shown in Fig. 7.

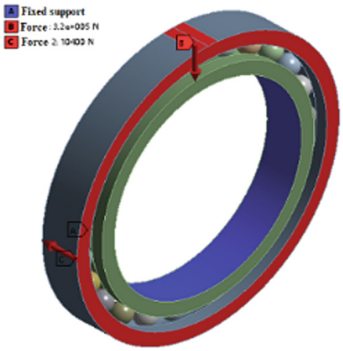

Fig. 7. Applied load constraint diagram

Simulation Results and Analysis

The analysis of the sixth-order modal results before the intercept loading simulation experiment, Table 3 shows the simulation data and the simulation results are shown in Fig. 8.

Table 3. Loading simulation experimental inherent frequency and maximum displacement

Number of steps	Frequency /Hz	Maximum displacement /mm	Vibration diagram
First step	2865.3	10.418	Figure 8-(a)
Second step	2991.1	23.465	Figure 8-(b)
Third step	3019.1	19.217	Figure 8-(c)
Fourth step	3120.3	19.179	Figure 8-(d)
Fifth step	3124.6	20.934	Figure 8-(e)
Sixth step	3221.6	17.237	Figure 8-(f)

As shown in Fig. 8, compared with the no-load simulation results, the first sixth-order mode vibration pattern of the loading simulation experiment is the same as that of the no-load simulation experiment. As can be seen from the sixth-order mode vibration diagram of the former loading simulation experiment, the maximum displacement is generated in the second-order mode, and the outer ring of the bearing is distorted in the axial direction, with the maximum displacement of 23.465 mm, corresponding to a frequency of 2991.1 Hz. The strength of the outer ring surface of the main bearing will directly affect the performance of the main bearing of the wind turbine.

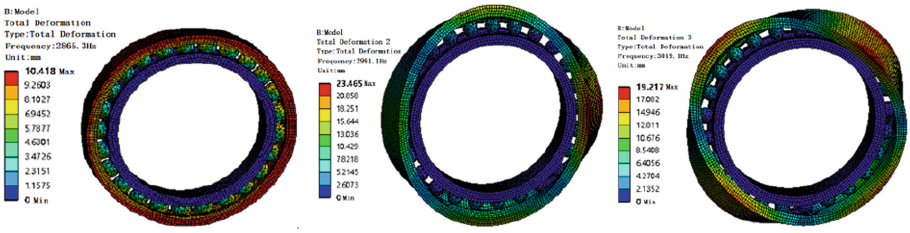

(a) First-step modal results (b) Second-step modal results (c) Third-step modal results

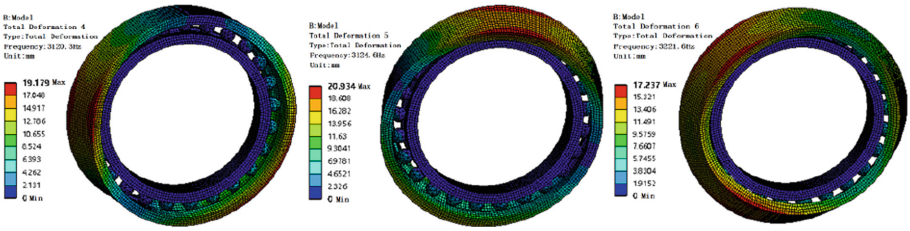

(d) Fourth-step modal results (e) Fifth-step modal results (f) Sixth-step modal results

Fig. 8. The first six orders of modal vibrations

From the information of the loaded simulation experimental solution scheme in Table 4, it can be seen that the first-order mode has the largest deformation variables in the Y-direction, Z-direction, and around the X-axis, corresponding to a fixed frequency of 2865.32 Hz. The sixth-order mode has the largest deformation variables in the X-direction and around the Y-direction, corresponding to a fixed frequency of 3221.60 Hz. The fifth-order mode has the largest deformation variables around the Z-axis, corresponding to a fixed frequency of 3124.65 Hz.

4.3 Data Analysis Comparison and Conclusion

The data from the unloaded modal analysis and the loaded modal analysis are compared as shown in the folded lines Fig. 9 and Fig. 10. It can be concluded that the maximum difference between the applied restraint and no-load state is 5 Hz, and the maximum difference of the maximum deformation is 0.73 mm. And according to the first six orders of the main bearing modal vibration, the winner bearing will produce deformation in a both no-load and loaded state, but the deformation mainly occurs in the axial direction, and the radial deformation is not obvious. According to the actual installation process, because there will be some dimensional constraints in the radial direction, the next axial vibration analysis simulation experiments of the constrained radial direction.

Table 4. No-load experiment solving scheme information

Number of steps	Frequency /Hz	RATIO
First step	2867.8	0.009834
Second step	2994.4	0.036612
Third step	3021.0	0.004127
Fourth step	3120.6	0.142800
Fifth step	3129.6	0.076644
Sixth step	3224.6	1.000000

(a) PARTICIPATION FACTOR CALCULATION_X DIRECTION

Number of steps	Frequency /Hz	RATIO
First step	2867.8	1.000000
Second step	2994.4	0.013960
Third step	3021.0	0.046589
Fourth step	3120.6	0.097306
Fifth step	3129.6	0.026198
Sixth step	3224.6	0.014898

(b) PARTICIPATION FACTOR CALCULATION_Y DIRECTION

Number of steps	Frequency /Hz	RATIO
First step	2867.8	1.000000
Second step	2994.4	0.023159
Third step	3021.0	0.012635
Fourth step	3120.6	0.030641
Fifth step	3129.6	0.136951
Sixth step	3224.6	0.049429

(c) PARTICIPATION FACTOR CALCULATION_Z DIRECTION

(*continued*)

Table 4. (*continued*)

Number of steps	Frequency /Hz	RATIO
First step	2867.8	1.000000
Second step	2994.4	0.003810
Third step	3021.0	0.003099
Fourth step	3120.6	0.006297
Fifth step	3129.6	0.000038
Sixth step	3224.6	0.007487

(d) PARTICIPATION FACTOR CALCULATION_ROTX DIRECTION

Number of steps	Frequency /Hz	RATIO
First step	2867.8	0.011747
Second step	2994.4	0.099362
Third step	3021.0	0.031977
Fourth step	3120.6	0.355309
Fifth step	3129.6	0.315969
Sixth step	3224.6	1.000000

(e) PARTICIPATION FACTOR CALCULATION_ROTY DIRECTION

Number of steps	Frequency /Hz	RATIO
First step	2867.8	0.013894
Second step	2994.4	0.030858
Third step	3021.0	0.035733
Fourth step	3120.6	0.739125
Fifth step	3129.6	1.000000
Sixth step	3224.6	0.219208

(f) PARTICIPATION FACTOR CALCULATION_ROTZ DIRECTION

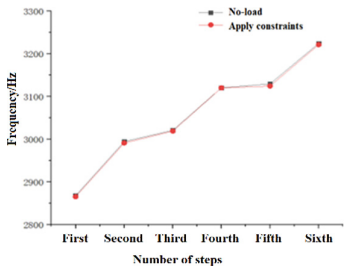

Fig. 9. Comparison of inherent frequency

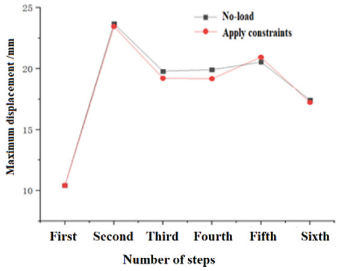

Fig. 10. Comparison of maximum deformation

5 Constrained Radial Axial Vibration Simulation Experiment

5.1 Determination of Working Conditions and Loads

The simulation experiment mainly observes the deformation of the main bearing of the wind turbine along the axial direction in different orders under no load, so the inner ring of the main bearing is fixed constrained, while the displacement of the outer ring of the main bearing excluding the axial direction is set to 0. The axial simulation experimental model constraint is shown in Fig. 11.

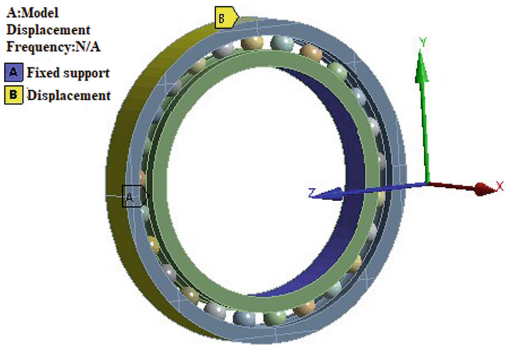

Fig. 11. Axial simulation experimental model constraint diagram

5.2 Simulation Results

The first six orders of modal results are intercepted and analyzed, Table 5 shows the simulation data, and the simulation results are shown in Fig. 12.

Table 5. Axial simulation experimental inherent frequency and maximum displacement

Number of steps	Frequency /Hz	Maximum displacement /mm	Vibration diagram
First step	5340.9	10.065	Figure 12-(a)
Second step	5661.1	13.931	Figure 12-(b)
Third step	5678	13.524	Figure 12-(c)
Fourth step	6553.9	13.682	Figure 12-(d)
Fifth step	6573	13.664	Figure 12-(e)
Sixth step	7837.6	13.557	Figure 12-(f)

As can be seen from the first six orders of mode vibration diagram, in the second order mode, the displacement of the main bearing along the axial scuttle is the largest, and the deformation is 13.931 mm, accounting for 24.9% of the main bearing thickness,

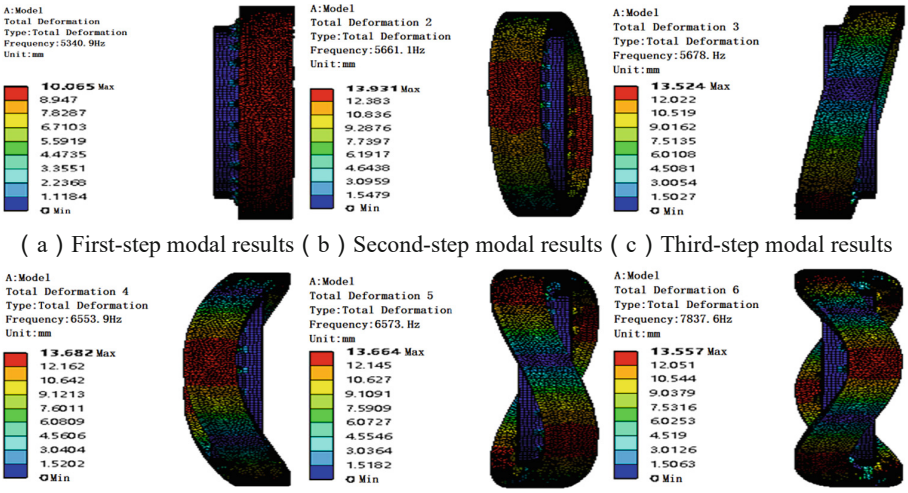

(a) First-step modal results (b) Second-step modal results (c) Third-step modal results

(d) Fourth-step modal results (e) Fifth-step modal results (f) Sixth-step modal results

Fig. 12. Sixth-order mode oscillation before the axial simulation experiment

corresponding to a frequency of 5661.1 Hz. The impact of axial deformation on the whole bearing is not negligible.

During the actual use of the main bearing of the wind turbine, the trend of its axial deformation will be translated into the restraining effect of the main shaft shoulder and end cover on it, and act on the bolt preload force, and the change of its axial force will affect the change of the bolt preload force. According to the first six orders of the main bearing modal vibration pattern and vibration frequency, it is known that the sampling frequency needs to reach about 10000 Hz, and the preload force of the bearing is inferred from the magnitude of the deformation.

6 Conclusion

Through the comparative analysis of the sixth-order vibration, pattern results under different modes of the wind power main bearing, it is obtained that the main vibration deformation of the wind power main bearing radially and axially in the operating condition occurs mainly in the axial direction, and the deformation in the radial direction has less influence. Further, the axial vibration experiments in the constrained radial direction are carried out, and the vibration characteristics of the main bearing along the axial scuttle are obtained, and the maximum deformation can reach 24.9% of the bearing thickness. This deformation will be restrained by the interaction force of the bearing with the end cap and spindle shoulder under actual working conditions. By monitoring the deformation of the main bearing in the axial direction, the operating condition of the main bearing can be monitored, and the magnitude of the preload force of the axial end cap bolts of the main bearing can be further analyzed to provide a theoretical basis for the selection of the parameters (range and signal sampling frequency) of the main bearing operating condition monitoring sensor.

Funding. This research was funded by China Postdoctoral Science Foundation, grant number 2021M692452, and Jiangsu Provincial Bureau of Market Regulation in China, grant number 2021SC64–4-35.

References

1. Xiao, X., Liu, J., Liu, D., Tang, Y., Qin, S., Zhang, F.: A normal behavior-based condition monitoring method for wind turbine main bearing using dual attention mechanism and Bi-LSTM. Energies **15**(22), 8462 (2022)
2. Yang, X., Zhang, T., Li, L., Wang, Y.Q.: Mechanical loading model of main bearing of wind turbine based on test bench. Eng. Appl. Sci. **6**(3), 55–65 (2021)
3. Li, Z.: A review of data-driven techniques for early bearing fault diagnosis. Mech. Trans. **47**(03), 165–176 (2023)
4. Wang, C., Chen, C., Wei, W.: Analysis of contact stress characteristics of wind turbine bearings under multivariable loads. Noise Vibr. Control **38**(S1), 108–111 (2018)
5. Huilan, L., Wan, Y.: Modal analysis of deep groove ball bearings based on ANSYS. Intern. Combust. Engine Accessories **323**(23), 56–57 (2020)
6. Hu, Q., Yang, X.: Multi-objective optimization design of angular contact ball bearings using sensitivity analysis. J. Huaqiao Univ. (Nat. Sci. Ed.) **41**(05), 555–560 (2020
7. Hu, Y., Dong, H., Mei, G., et al. Mechanical analysis of a new single-point mooring spherical plain bearing. Bearings **476**(07), 11–15 (2019)
8. Liu, Z., Zou, H., Miao, H., Chen, D., Zang, C.: Confirmation of kinetic model of on-load tap-changer components based on super model. Mach. Manufact. Autom. **48**(05), 131–135 (2019)
9. Zhao, T., Ma, P., Xu, N.: Optimization analysis of response surface of shallow buried pipe after dam based on ANSYS Workbench. Hydroelectr. Power, **44**(04), 29–32+115 (2018)
10. Wu, Z., Liu, J., Ran, L., Ye, J.: Dynamic stress analysis and structural optimization of horizontal sieve body based on ANSYS Workbench. Equip. Manufactur. Technol. **09**, 43–47 (2020)
11. Zhao, Z.: Application of ANSYS workbench-based software in bearing housing modal analysis. Explosion-proof Electr. Mach. **57**(01), 27–28+42 (2022)